

Article

A Quantitative Analysis of the Influence of Temperature Change on the Extreme Precipitation

Wei Zhu ^{1,2} , Shuangtao Wang ^{1,2}, Pingping Luo ^{1,2,*} , Xianbao Zha ^{1,2}, Zhe Cao ^{1,2}, Jiqiang Lyu ^{1,2} ,
Meimei Zhou ^{1,2}, Bin He ³ and Daniel Nover ⁴

¹ Key Laboratory of Subsurface Hydrology and Ecological Effects in Arid Region, Ministry of Education, Chang'an University, Xi'an 710054, China; 2020029006@chd.edu.cn (W.Z.); 2019029018@chd.edu.cn (S.W.); 2019129068@chd.edu.cn (X.Z.); 2019129022@chd.edu.cn (Z.C.); lvjiqiang0721@chd.edu.cn (J.L.); mmzhou@chd.edu.cn (M.Z.)

² School of Water and Environment, Chang'an University, Xi'an 710054, China

³ National-Regional Joint Engineering Research Center for Soil Pollution Control and Remediation in South China, Guangdong Key Laboratory of Integrated Agro-Environmental Pollution Control and Management, Institute of Eco-environmental and Soil Sciences, Guangdong Academy of Sciences, Guangzhou 510650, China; bhe@soil.gd.cn

⁴ School of Engineering, University of California Merced, 5200 Lake R, Merced, CA 95343, USA; dmnover@gmail.com

* Correspondence: lpp@chd.edu.cn; Tel.: +86-2982339376

Abstract: As an essential part of the hydrological cycle, precipitation is usually associated with floods and droughts and is increasingly being paid attention to in the context of global warming. Analyzing the change trends and correlation of temperature and extreme precipitation indicators can effectively identify natural disasters. This study aimed to detect the correlation and change trends of temperature and extreme precipitation indicators in Inner Mongolia from 1960 to 2019. Panel vector autoregression (PVAR) models based on Stata software were used to detect the correlation between temperature and extreme precipitation indicators at 35 climatological stations throughout Inner Mongolia. The temperature and extreme precipitation indicator trends were analyzed using the Mann–Kendall test and Sen's slope method. The spatial distribution characteristics of the annual precipitation and rainfall intensity were more significant in the southeast and more minor in the northwest, while an increase in the annual wet days was noticeable to the northeast. The Granger cause tests of the temperature and the extreme precipitation indicators showed a correlation between each indicator and temperature at the significance level of 1%. The temperature positively correlated with only the rainfall intensity while negatively correlating with the remaining indicators. There is no doubt that trend analysis showed significant increasing trends in rainfall intensity at all stations, which means increased risk in extreme precipitation events. By contrast, the annual precipitation and annual wet days showed significant decreasing trends, which means that the precipitation is concentrated, and it is easier to form extreme precipitation events. The study can provide a basis for decision-making in water resources and drought/flood risk management in Inner Mongolia, China.

Keywords: extreme precipitation events; climate change; PVAR models; Mann–Kendall test



Citation: Zhu, W.; Wang, S.; Luo, P.; Zha, X.; Cao, Z.; Lyu, J.; Zhou, M.; He, B.; Nover, D. A Quantitative Analysis of the Influence of Temperature Change on the Extreme Precipitation. *Atmosphere* **2022**, *13*, 612. <https://doi.org/10.3390/atmos13040612>

Academic Editor: Tomeu Rigo

Received: 16 March 2022

Accepted: 7 April 2022

Published: 11 April 2022

Publisher's Note: MDPI stays neutral with regard to jurisdictional claims in published maps and institutional affiliations.



Copyright: © 2022 by the authors. Licensee MDPI, Basel, Switzerland. This article is an open access article distributed under the terms and conditions of the Creative Commons Attribution (CC BY) license (<https://creativecommons.org/licenses/by/4.0/>).

1. Introduction

Extreme precipitation is one of the most severe natural disasters, leading to enormous economic losses worldwide [1]. In recent decades, extreme precipitation events have been extensively researched worldwide, such as in China, India, North America, South America, Africa, Europe, and Australia [2]. The magnitude and frequency of extreme precipitation events are expected to increase in the near future, especially at sub-daily timescales, which may lead to more natural disasters such as riverine floods, flash floods, and landslides [3,4]. Compared to a single extreme precipitation event, compound extremes related to floods

and droughts may aggravate the influence on the environment and society [5]. Therefore, it is necessary to thoroughly understand the magnitude, duration, and frequency of extreme precipitation events for the effective design, planning, and management of these systems [6].

In order to address the challenges of extreme precipitation events, it is necessary to implement ecologically sound and sustainable measures based on scientific information [7]. In detail, the nature and extent of the extreme precipitation-related indicators need to be further studied [8]. This research is considered essential for developing management policies and assessing the natural and social impacts of extreme precipitation events. In addition, knowledge about extreme precipitation events is vital for everyday life, as it plays an essential role in the management and the response of emergencies [9]. Recently, the extreme precipitation events analysis at a particular area has paid considerable attention mainly due to its influences for risk management and hazard assessment, especially related to drought/flood disasters [10].

The simulation and projection of temperature and extreme precipitation events have been extensively studied worldwide [11]. Changes in temperature and extreme precipitation events have also been researched in China [12], in the Caribbean [13], in the Southern Pacific [14], and in Africa [15]. Some scholars have researched extreme events of combinations of precipitation and temperature over the past several years and found that the number of extreme events increased rapidly on a global scale [16]. Extreme precipitation events also affect precipitation patterns and water balance and accelerate desertification. Therefore, it can profoundly impact ecosystems and human society [17]. The study shows that analysis based on univariate events that are related to each other may underestimate the risks of compound extremes [18]. These studies show that, with global climate change and human activities, the risk of extreme precipitation events increases significantly in future periods.

China is a country with vast land territory, which occupies a significant portion of the world. The publication of many scholars shows that China's climate is highly affected by the East Asian summer monsoon [19]. Since conditions geographical and meteorological are considerably complex and diverse in China, the changes of the extreme precipitation events have been studied by researchers in recent years [20], identifying changes in regional extreme precipitation events in order to support disaster prevention and policy development in specific regions. Some researchers provide a valuable tool for calling attention to the local government and contributing to global research by comparing China's results with those of other parts of the world [21]. In the past decades, the tendency to increase extreme precipitation has been significant in the middle and lower reaches of the Yangtze River, Western and Southwestern China, and some coastal areas of Southern China. In contrast, the decreasing trend of extreme precipitation appears in the northern regions [22]. The extent to which the changes in the temperature and precipitation-related indices affects the total amount of extreme precipitation events over China in the present climate has not yet been assessed. Moreover, how will this influence change in the near future over China? The present study addresses these questions by analyzing the observational and model simulation data [23].

Some scholars have pointed out significant changes in indicators that have characterized the frequency and intensity of extreme precipitation events in the past 10 years [24]. The research on extreme precipitation events in China mainly aims at the whole country or large areas in the north. However, there is little research on extreme precipitation events in Inner Mongolia. The terrain of Inner Mongolia is complex, spanning Northwest China, North China, and Northeast China from east to west. The uncertainty and variability introduced by the complex terrain can be associated with the significant error in precipitation estimates [25–27]. The annual precipitation in this area is small and uneven, mainly concentrated in the summer, resulting in frequent droughts and floods, seriously affecting the production of agriculture and animal husbandry and people's lives [28]. Due to global warming, the temperature of the whole region has increased significantly in the past 60 years [29]. Some researchers have found no significant increase or decrease

in the average summer precipitation and annual precipitation extreme events in Inner Mongolia. However, after entering the 21st century, the extreme precipitation events from July to August decreased significantly [30,31]. However, previous studies have focused on extreme precipitation changes, and there are few studies on the response to climate change, especially the relationship between extreme precipitation and temperature. Therefore, this work further studies the temporal and spatial variations of extreme precipitation in Inner Mongolia to understand better the impact of global climate change there.

This study aimed to detect the correlation and change trends of temperature and extreme precipitation indicators in Inner Mongolia from 1960 to 2019. The research must help understand the nature of climatic phenomena and assess the changes and impacts of extreme precipitation events on the future climate. The remainder of this paper proceeds as follows: Firstly, Section 2 provides a comprehensive description of the main characteristics of the study area. Secondly, the materials and methods, the results of the investigation, and a discussion are provided. Finally, Section 6 summarizes the conclusions obtained from this research.

2. Study Area

Inner Mongolia is located within Eurasia, with a temperate continental climate, across Northeast, North, and Northwest China between $97^{\circ}12' \sim 126^{\circ}04'$ east longitude and $37^{\circ}24' \sim 53^{\circ}23'$ north latitude (Figure 1). It covers an area of about 1.183 million squares kilometers, accounting for 12.3% of China's land area, and is the third-largest province in China. The topography slopes from northeast to southwest, showing a narrow shape, and most of the whole region belongs to a high prototype geomorphological area. Inner Mongolia is the province with the largest number of neighboring provinces in China, with eight provinces bordering it (Heilongjiang, Jilin, Liaoning, Hebei, Shanxi, Shaanxi, Ningxia, and Gansu Province).

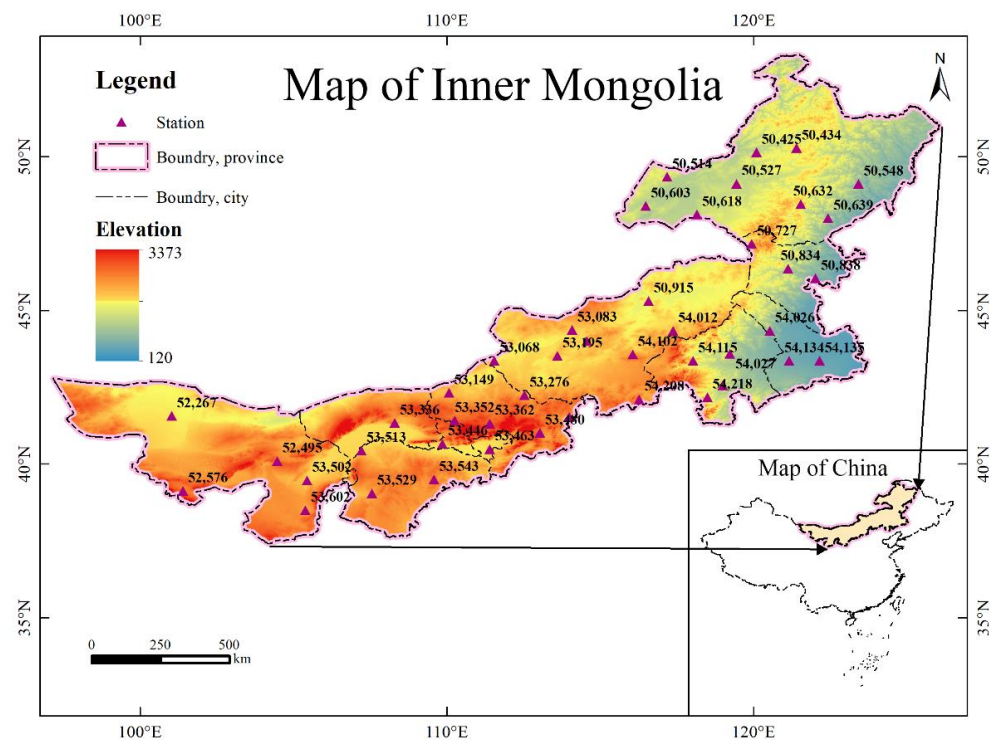


Figure 1. Study area and observed meteorological stations.

The average elevation of Inner Mongolia is about 1000 m. The highest elevation of Inner Mongolia is 3556 m at the Ho-lan Mountains. Inner Mongolia has a vast territory, high latitude, large plateau area, far away from the sea, and mountains along the border, and the climate is dominated by a temperate continental monsoon climate. Figure 2 shows

the Köppen–Geiger climatic zones of Inner Mongolia. It has the characteristics of less and uneven precipitation, strong wind, and drastic temperature changes.

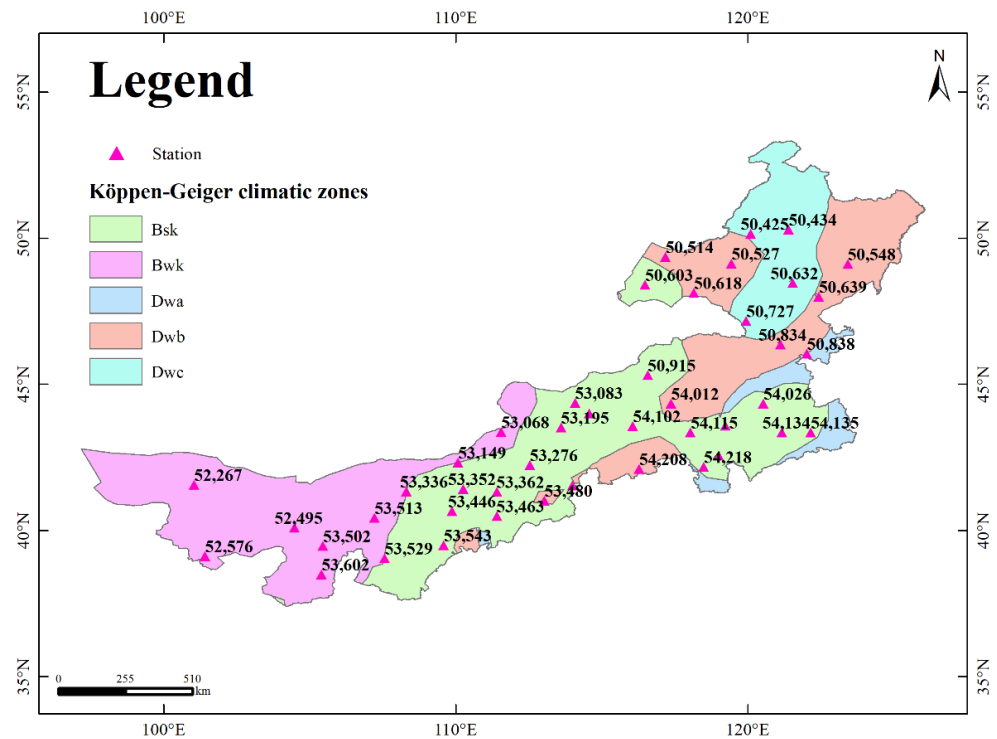


Figure 2. The Köppen–Geiger climatic zones of the study area.

The annual average precipitation in Inner Mongolia is between 219 and approximately 452 mm (Figure 3a). The precipitation from May to September, June to September, July to August, and monthly maximum precipitation generally account for about 70%, 60%, 30–80%, and 20–60% of the annual precipitation, respectively. The distribution of precipitation during the year is hugely uneven (Figure 3b). Inner Mongolia has abundant sunshine and light energy resources, and the annual sunshine hours in most areas are more than 2700 h. The average number of gale days in the year is about 10–40 days, and 70% occur in the spring.

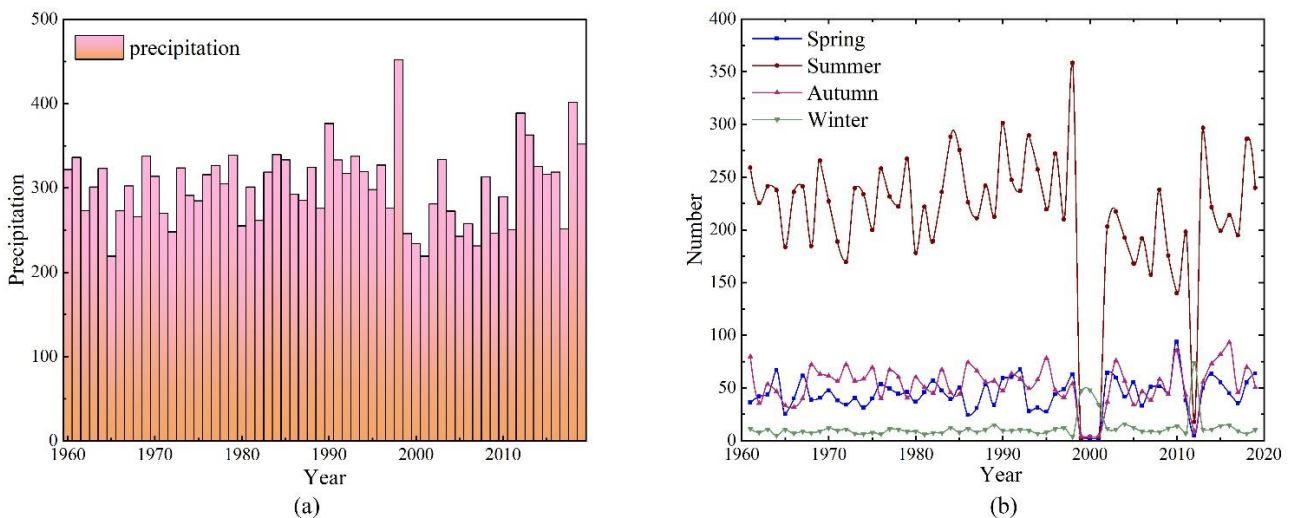


Figure 3. (a) The time series for the annual precipitation of the study area. (b) The time series for the precipitation for different seasons.

3. Materials and Methods

3.1. Materials

In this research, the daily total precipitation and temperature data during 1960–2019 of 44 stations in Inner Mongolia were extracted from the Daily Terrestrial Climatological Dataset in China (V3.0) released by the National Meteorological Information Center (<http://data.cma.cn/>, accessed on 16 September 2021). In order to ensure the quality of the data, it was checked and controlled before releasing. Based on the available meteorological records, stations with the records starting from 1960 and the percentage of missing values being less than 5% were selected. Finally, data from 44 stations were selected as survey samples, of which 35 stations collected data from 1960 to 2019 and 9 stations collected data from 1960 to 2017.

3.2. Method

3.2.1. Extreme Climate Indices

In order to effectively reflect the change in climate, the Expert Team on Climate Change Detection and Indices (ETCCDI) recommended 27 indices based on precipitation and temperature data [32]. Based on the analysis of previous research [33–35], this study selected the annual average temperature and 3 extreme climate indices (PRCPTOT, SDII, and Wet Days) for analysis (Table 1). The program is developed based on the Fortran language to calculate these extreme precipitation indicators.

Table 1. Extreme climate indices.

Indices	Definitions	Units
Temperature	Annual average temperature	°C
PRCPTOT	Annual total precipitation in wet days	mm
Wet Days	Annual count of days when rainfall ≥ 1 mm	day
SDII	Annual total precipitation divided by the number of wet days in the year	mm/day

3.2.2. PVAR Models

Time series vector autoregression (VAR) models first appeared in econometrics as a substitute [36,37]. With the introduction of VAR models in panel data settings, panel vector autoregression (PVAR) models have been more and more used in the applied study across fields [38]. The PVAR model regards the study variables as endogenous variables, a function of the lag values of all endogenous variables, to obtain more data characteristics. It is represented by the following equations:

$$Y_{it} = \alpha_{i0} + \sum_{j=1}^p \alpha_{ij} Y_{i,t-j} + \gamma_i + \theta_t + \varepsilon_{it} \tag{1}$$

where Y_{it} represents the endogenous variable of the i station in the t year; j represents a lag value; and γ_i , θ_t , and ε_{it} are unit effects, time effects, and idiosyncratic errors, respectively.

The settings of the PVAR models with which the cross-sectional units share the same underlying data-generating process contrasts with the VAR models. In the PVAR models, the parameters are estimated as distributions. In the VAR models, the parameters are specific to the unit being studied.

The unit root test has become routine to process panel data. The method of unit root testing mainly includes the LLC unit root test [39], IPS unit root test [40], Breitung unit root test [41], and Fisher unit root test [42]. The LLC unit root test is used to test the null hypothesis of a common unit root in the panel against the alternative of stationarity when cross-sectional units are independent on each other [43]. The IPS unit root test combines the evidence on the unit root hypothesis from the n unit root tests performed on the n cross-section units [44]. The Breitung unit root test compared the robust Dickey–Fuller t -statistics under contemporaneously correlated errors with the GLS t -statistics based on the transformed model [41]. The Fisher unit root test is the inverse chi-square test and is most widely used in meta-analyses [42].

In addition, the PVAR models require selecting the optimal lag order. For this purpose, we relied on the moment and model selection criteria (MMSC) for the generalized method of moments (GMM) models [45]: the Bayesian information criterion (MBIC), the Akaike information criterion (MAIC), and the Hannan–Quinn information criterion (MQIC) [46].

3.2.3. Spatial Interpolation

The Kriging algorithm is a robust statistical interpolation method for diverse applications such as geochemistry, health sciences, and pollution modeling [47]. Therefore, this study used the kriging algorithm for spatial interpolation.

There are several types of the Kriging algorithm. The most common method is Ordinary Kriging, which assumes that the data have no constant mean over an area mean (no trend). In comparison, Universal Kriging does assume that the data have an overriding trend and that it can be modeled [47].

Although only Kriging interpolation was used in this study, previous studies have found no significant differences between the simplest Kriging method and the most complex geostatistics, with satisfactory general results [48,49].

3.2.4. Mann–Kendall (MK) Test and Sen’s Trend Estimator

The MK test is a nonparametric test mainly used to analyze long-term trends of temperature, precipitation, and runoff [50,51]. Compared with parametric statistics, its advantage is less sensitive to outliers and does not need normality or linearity assumptions. Under the assumption that the time series x_n has no trend, the statistical S test is given as follows:

$$S = \sum_{i=1}^{n-1} \sum_{j=i+1}^n \text{sgn}(x_j - x_i) \tag{2}$$

where n is the number of sample points, x_i and x_j are the data values in the time series i and j ($j > i$), and $\text{sgn}(x_j - x_i)$ is given as follows:

$$\text{sgn}(x_j - x_i) = \begin{cases} +1, & x_j - x_i > 0 \\ 0, & x_j - x_i = 0 \\ -1, & x_j - x_i < 0 \end{cases} \tag{3}$$

The variance value of S is as follows:

$$\text{Var}(S) = \frac{n(n-1)(2n+5) - \sum_{i=1}^n t_i(t_i-1)(2t_i+5)}{18} \tag{4}$$

The normal approximation Z test is written as follows:

$$Z = \begin{cases} \frac{S-1}{\sqrt{\text{Var}(S)}} & \text{if } S > 0 \\ 0 & \text{if } S = 0 \\ \frac{S+1}{\sqrt{\text{Var}(S)}} & \text{if } S < 0 \end{cases} \tag{5}$$

Note that the significance of a trend is evaluated using the standardized test statistic (Z) value. This study tests for either an upward or downward trend at the $\alpha = 0.05$ level of significance ($Z_{1-\alpha/2} = 1.96$), and positive and negative Z values indicate increasing and decreasing trends. H_0 is rejected if $|Z| > Z_{1-\alpha/2}$; otherwise, there is no significant data trend. Sen’s estimator is a robust linear regression method that detects the magnitude of these increasing and decreasing trends of sample points [52].

4. Results

It can be shown that the spatial distribution of the mean PRCPTOT in Inner Mongolia during the period from 1960 to 2019 was obtained using Kriging interpolation based on ArcGIS software (ESRI, Redlands, CA, USA) (Figure 4). The spatial distribution characteristic of the mean PRCPTOT of the stations in Inner Mongolia exhibits an increasing trend from

northwest to southeast, and there is a significant gap between the maximum and minimum. The minimum of the mean PRCPTOT is observed at Ejinaqi Station as 35 mm, while the maximum is 509 mm at Xiaoergou Station. The spatial difference of the mean PRCPTOT in Inner Mongolia is affected by climate, latitude, geography, and geomorphology. There is a significant difference in the mean PRCPTOT between the southern and northern foothills of the Yin Mountains. The humid air in the south is blocked by the Yin Mountains, resulting in less rainfall north of the Yin Mountains.

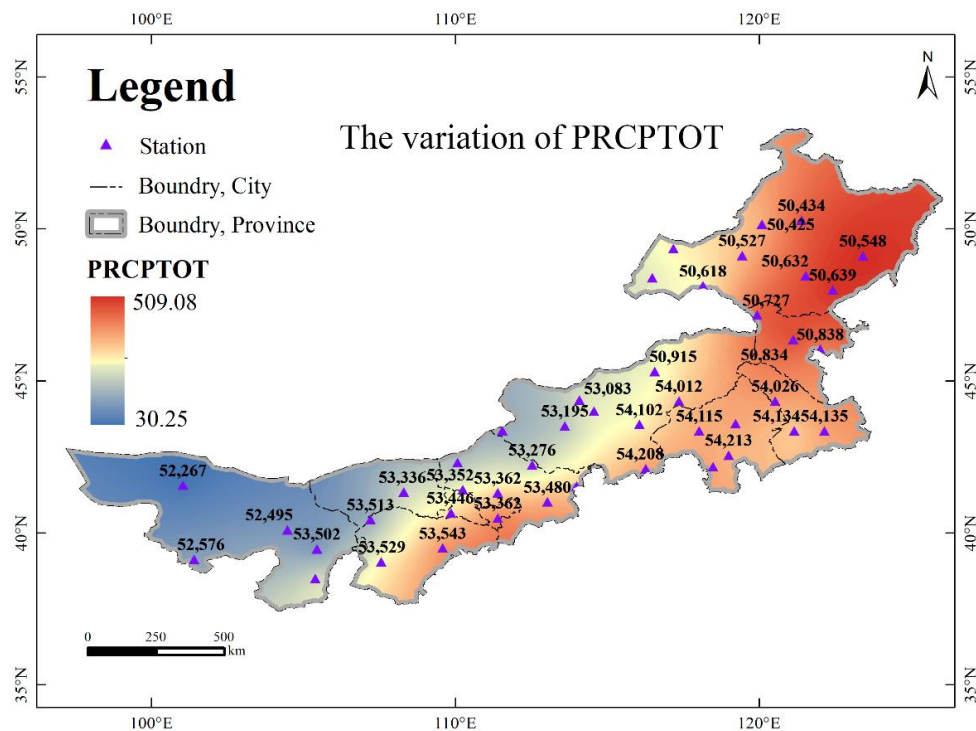


Figure 4. Spatial distribution of the mean PRCPTOT.

The spatial distribution of the mean wet days in Inner Mongolia during the period from 1960 to 2019 is exhibited in Figure 5. The minimum of the mean wet days is also observed at Ejinaqi Station as 18 days, while the maximum is 153 days at Aershan Station. Unlike the spatial distribution characteristic of the mean PRCPTOT, the maximum of the mean wet days is concentrated in the northeast of Inner Mongolia. The mean wet days in Southeastern Inner Mongolia is at a low level, but the mean PRCPTOT is at a high level, which leads to a higher mean SDII more prone to extreme precipitation events.

The spatial distribution of the mean SDII in Inner Mongolia during the period from 1960 to 2019 is exhibited in Figure 6. The minimum of the mean SDII is also observed at Ejinaqi Station as 1.93 mm/day, while the maximum is 5.99 mm/day at Zhalute Station. The variation trend of the spatial distribution of the mean SDII is consistent with that of the spatial distribution of the mean PRCPTOT, and the maximum of SDII in Southeastern Inner Mongolia proves the previous inference. Similarly, there is a significant difference in the mean SDII between the southern and northern foothills of the Yin Mountains. Under the influence of the monsoon, the moist air reaching the southern foothill of the Yin Mountains is lifted by the terrain during air movement. With the increase of altitude, the water vapor cools to form precipitation, making the precipitation at the southern foothill of the Yin Mountains higher than the northern foothill of the Yin Mountains.

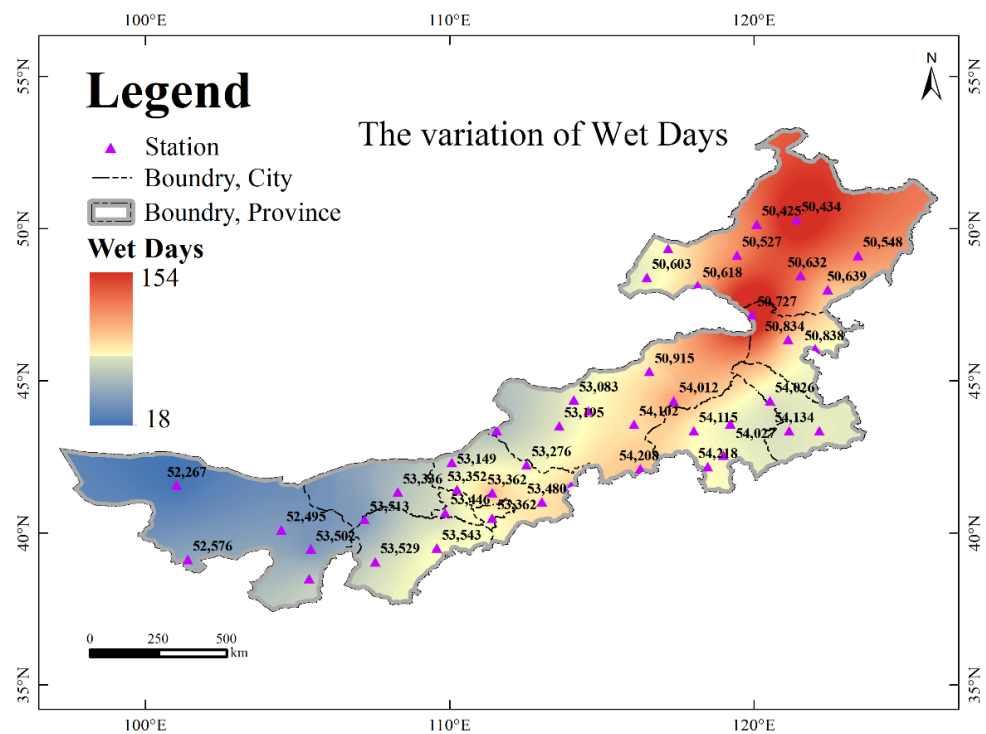


Figure 5. Spatial distribution of the mean wet days.

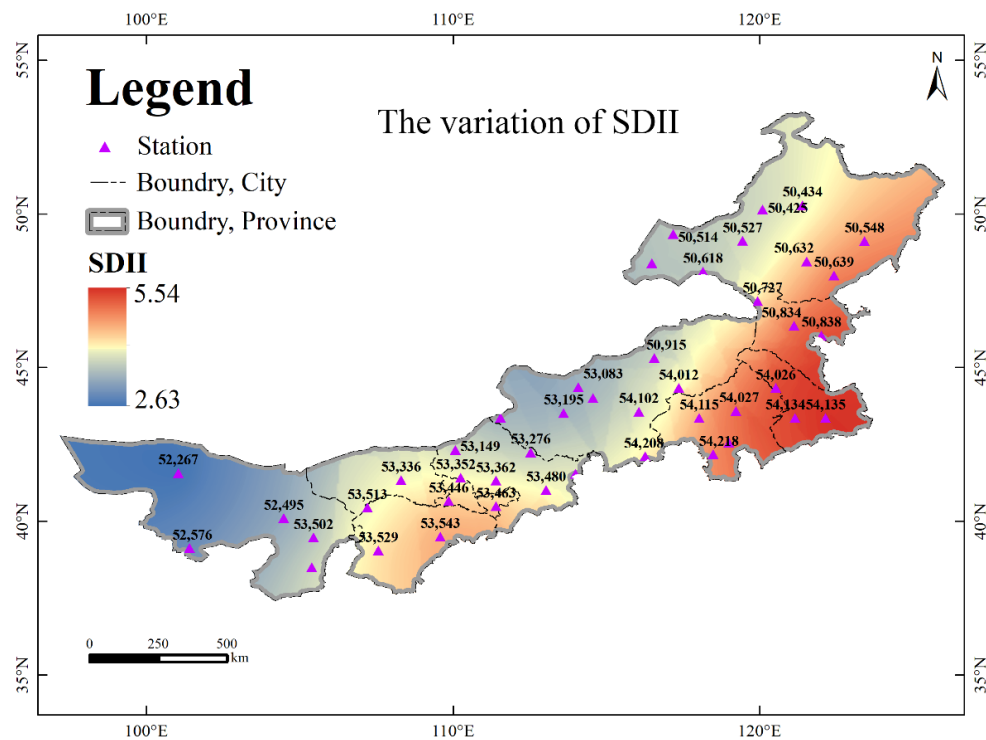


Figure 6. Spatial distribution of the mean SDII.

In order to understand the essential characteristics of the study data, descriptive statistics (Table 2) provide the standard deviation; minimum, maximum, and mean for temperature; and other extreme precipitation indicators. Overall represents that all the statistical data of 2100 observations are used for calculation. Between represents that the results are calculated based on the statistical data of 35 stations regardless of time. Within

represents that the results are calculated using the statistical data of 60 years regardless of stations.

Table 2. Descriptive statistics of the study variables.

Variable		Mean	Std. Dev.	Min	Max	Observations
Temperature	overall	3.4853	3.3381	−6.71	10.34	N = 2100
	between		3.2463	−4.3323	8.1197	n = 35
	within		0.9489	0.8457	5.97	T = 60
PRCPTOT	overall	325.3502	127.5773	39.7	1111.5	N = 2100
	between		93.5182	137.0217	509.175	n = 35
	within		88.1824	34.7202	932.9202	T = 60
Wet Days	overall	77.5557	25.1283	21	205	N = 2100
	between		22.9522	36.0333	153.75	n = 35
	within		10.9286	36.8057	128.8057	T = 60
SDII	overall	4.2781	1.4414	1.28	11.54	N = 2100
	between		1.0011	2.8538	5.9875	n = 35
	within		1.0506	0.9766	11.0829	T = 60

The concepts of “spurious regression” and “spurious correlation” could appear between independent unit root variables. Therefore, for panel data, we should first carry out a unit root test for each variable in the panel—that is, the stationarity test of variables. The method of the unit root test mainly included the LLC unit root test, IPS unit root test, Breitung unit root test, and Fisher unit root test. In order to ensure the reliability of the conclusions, this study comprehensively used the above four methods to test the stationarity of the temperature and other extreme precipitation indicators and then judged the stationarity of the variables (Table 3). The research showed that all variables were stationary sequences at the significance level of 5%, and all sequences contained drift terms and trend terms.

Table 3. Unit root test.

Variables	LLC	IPS	Breitung	Fisher-ADF
Temperature	−30.9737 ***	−28.0859 ***	−1.4916 **	168.3305 ***
PRCPTOT	−44.4018 ***	−41.2530 ***	−4.5287 ***	355.0586 ***
Wet Days	−37.9387 ***	−36.7455 ***	−3.9278 ***	249.3556 ***
SDII	−43.9659 ***	−40.5206 ***	−3.9635 ***	306.1874 ***

Note: ** and *** represent the significance levels of 5% and 1%, respectively.

The optimal lag order is selected by the MBIC, MAIC, and MQIC. In the study, the optimal lag order of the model is selected to be 5 using Stata software. According to the test of the eigenvalue stability condition of the model, it was found that all eigenvalues of the PVAR models were inside the unit circle, indicating that the PVAR models had a high degree of stability. The paper researched the Granger cause equation between temperature and other extreme precipitation indicators. The results showed that all H_0 were rejected besides the fact that SDII is not a Granger cause Equation variable (Table 4). Therefore, the research shows Granger reasons between temperature and other extreme precipitation indicators. That is, the temperature will exert influence on the extreme precipitation indicators.

According to the correlation matrix of all the study variables (Table 5), the temperature had a positive correlation with only SDII and a negative correlation with the remaining variables. It was also found from the correlation matrix that all study variables were correlated at the significance level of 1%. It represented a highly negative correlation of the correlation coefficient of the temperature and wet days over 0.7.

Table 4. Panel VAR Granger causality Wald test.

Null Hypothesis (H ₀)	F-Statistics	p-Value	Conclusion
Temperature is not a Granger cause equation variable	20.375	0.001	Rejection
PRCPTOT is not a Granger cause equation variable	17.540	0.004	Rejection
Temperature is not a Granger cause equation variable	41.208	0.000	Rejection
Wet Days are not Granger cause equation variables	20.713	0.001	Rejection
Temperature is not a Granger cause equation variable	45.216	0.000	Rejection
SDII is not a Granger cause equation variable	7.737	0.171	Acceptance

Table 5. Correlation matrix.

Variables	Temperature	PRCPTOT	Wet Days	SDII
Temperature	1			
PRCPTOT	−0.183 ***	1		
Wet Days	−0.720 ***	0.552 ***	1	
SDII	0.401 ***	0.689 ***	−0.178 ***	1

Note: *** represent the significance levels of 1%.

The study shows the MK trend test distributions of all variables from 1960 to 2019 (Table 6). The temperatures at all stations showed significant increasing trends, and there is no doubt that the climate is gradually warming. We were surprised to find that the PRCPTOT of almost all stations exhibited no significant trend, and only Manzhouli was detected to have a decreasing trend. According to the above correlation matrix results, it is inferred that the PRCPTOT in Inner Mongolia may show a downward trend in the future. The wet days of most stations also exhibited no significant trend, and only the wet days of one out of five stations were detected to have a decreasing trend. Interestingly, most of these stations were located in the eastern part of Inner Mongolia. The SDII of seven stations detected a significant increasing trend, but two stations exhibited a decreasing trend, which was worthy of further study, and the rest stations showed no significant trends. In a word, the SDII of some stations were detected to have increasing trends, and it can be indicated that the extreme precipitation events are increasingly severe.

Table 6. Z Value and slope estimates.

Station	Temperature		PRCPTOT		Wet Days		SDII	
	Z	Sen	Z	Sen	Z	Sen	Z	Sen
Eerguna	−2.268	0.039	−0.836	−0.485	−0.166	0	−0.249	−0.001
Tulihe	4.981	0.033	−0.434	−0.222	−5.166	−0.556	2.398	0.011
Manzhouli	3.89	0.028	−2.289	−1.162	0.357	0.036	−2.041	−0.016
Hailaer	4.719	0.039	−0.242	−0.123	−1.486	−0.147	1.792	0.01
Xiaoergou	6.339	0.048	1.512	1.112	−4.369	−0.458	3.852	0.031
Xinbaerhuyouqi	5.134	0.037	−1.237	−0.811	0.549	0.041	−1.677	−0.015
Xinbaerhuzuoqi	5.102	0.038	0.383	0.154	0.823	0.063	0.268	0.002
Zhalantun	5.236	0.035	1.549	1.497	0.855	0.069	0.561	0.006
Aershan	5.096	0.032	0.542	0.407	−4.216	−0.457	2.283	0.011
Suolun	5.185	0.03	0.166	0.148	−0.708	−0.063	0.542	0.004
Dongwuzhumuqinqi	5.899	0.044	0.006	0.003	0	0	0.325	0.002

Table 6. Cont.

Station	Temperature		PRCPTOT		Wet Days		SDII	
	Z	Sen	Z	Sen	Z	Sen	Z	Sen
Erliahaote	5.638	0.048	0.434	0.149	−1.365	−0.092	0.721	0.005
Narenbaolige	5.791	0.047	−0.14	−0.097	−0.88	−0.077	0.306	0.001
Mandula	5.708	0.037	1.014	0.392	−0.804	−0.053	1.843	0.011
Abagaqi	5.938	0.049	−0.517	−0.2	−0.191	0	−0.364	−0.002
Wulatezhongqi	6.971	0.048	0.899	0.433	−0.842	−0.052	1.677	0.013
Damaoqi	6.333	0.044	0.874	0.457	−1.677	−0.111	2.341	0.011
Siziwangqi	5.772	0.039	1.371	0.861	0.319	0	1.69	0.009
Huade	6.327	0.041	0.051	0.031	−0.472	−0.045	0.057	0.001
Baotou	6.027	0.038	0.414	0.29	−0.568	−0.036	1.582	0.016
Hohhot	6.244	0.043	0.491	0.594	0.121	0	0.829	0.008
Jining	6.039	0.036	0.134	0.052	−1.544	−0.127	1.25	0.01
Linhe	6.448	0.048	0.204	0.088	0.887	0.056	−0.369	−0.003
Eketuoqi	5.466	0.031	0.427	0.269	0.019	0	0.593	0.007
Dongsheng	7.111	0.051	0.019	0.025	−0.976	−0.078	1.142	0.012
Xiwuzhumuqinqi	5.019	0.033	−0.299	−0.203	0.561	0.061	−1.033	−0.006
Zhalute	6.225	0.039	−0.319	−0.254	−0.95	−0.078	0.083	0.001
Balinzuoqi	6.697	0.047	0.427	0.218	−1.837	−0.105	1.199	0.012
Xilinhaote	5.676	0.041	−0.338	−0.239	0.549	0.054	−0.918	−0.006
Linxi	4.745	0.024	−0.899	−0.607	−0.599	−0.052	−0.816	−0.006
Kailu	5.785	0.035	−0.338	−0.213	0.013	0	−0.159	−0.002
Tongliao	6.269	0.041	−0.274	−0.163	−2.003	−0.152	0.281	0.003
Duolun	6.123	0.04	0.587	0.334	−1.416	−0.143	1.62	0.01
Wengniuteqi	4.618	0.025	−0.364	−0.304	−1.461	−0.11	0.268	0.002
Chifeng	4.095	0.02	0.395	0.238	−1.703	−0.125	1.767	0.014

5. Discussion

The spatial distribution of the extreme precipitation indicators (PRCPTOT, Wet Days, and SDII) in Inner Mongolia tends to be maximum in the southeast and minimum in the northwest. The results are consistent with the research in Inner Mongolia publicized by other scholars [53].

The research used panel data and a time-series data analysis technique to test the general theory by examining the correlation between the temperature and three extreme precipitation-related indicators in the past. The previous research suggests that extreme precipitation events have become increasingly severe with global warming [54,55]. Therefore, we detect causality for temperature and extreme precipitation indicators PRCPTOT, Wet Days, and SDII. Our findings suggest that the decreasing trend in PRCPTOT and wet days is accompanied by increases in the temperature. In contrast, the other type of relationship exhibited an increasing trend in SDII with increasing temperature. A station with the first relationship between PRCPTOT and temperature means an increased risk of drought or/and flood disaster events at the station. In addition, the station of the first relationship between PRCPTOT and temperature occurred in Northeastern Inner Mongolia. The climate characteristics of Inner Mongolia are very dry, and the annual precipitation is relatively small. Therefore, there is a greater risk of drought for the stations that showed the first type of relationship between PRCPTOT and temperature in the dry season. Due to the small wet days, the more concentrated the rainfall, the more flood disasters are caused. The second relationship between SDII and temperature means that flood disasters are becoming more and more frequent. Therefore, flood prevention should be paid attention to at some stations, such as Tulihe, Xiaoergou, and Chifeng.

Regarding temperature and extreme precipitation-related indicators from 1960 to 2019, PRCPTOT and wet days were mainly observed in decreasing trends across Inner Mongolia. Some scholars showed that the increasing trends of PRCPTOT aggravate the hazard of flooding, because a large amount of precipitation indicates an incidence of torrential rain. On the contrary, the decreasing trend of PRCPTOT indicates that more dry periods could

be detected [56]. However, SDII has shown a significant increasing trend in some stations in Inner Mongolia, such as Tulihe, Xiaoergou, and Aershan, which indicates that we should pay attention to the growing number of extreme precipitation events. At the same time, the present study shows that the decline rate of PRCPTOT in most stations was not as fast as that of wet days, which proves once again that extreme precipitation events are becoming more and more frequent. For temperature, all stations observed significant increasing trends in line with the current global warming situation. Some scholars suggested that changes in extreme climate events in most parts of the world are amplified at the tails, such as increases in extremely high temperatures, decreases in extremely low temperatures, and increases in extreme precipitation events [10]. In summary, the extreme precipitation events in Inner Mongolia have exhibited increasing trends, but precipitation is detected in decreasing trends.

The reduction of precipitation will significantly affect the ecosystem, the hydrological cycle, and the water supply of society. In detail, changes in precipitation will cause changes in runoff and groundwater to affect the hydrological cycle, which, in turn, affects the water supply and ecological environment. For agriculture, one of the most critical industries in China, the reduction of precipitation leads to a lack of soil moisture, greatly influencing crops. As far as hydropower projects are concerned, the influence of runoff change is very critical. In addition, the changes in extreme precipitation events are particularly significant for managing water resources, the formulation of flood control policies, the reduction of soil erosion, and the acquisition of natural water resources [57,58]. Ultimately, the changes of extreme precipitation events will significantly influence the ecosystem and human society of the whole of Inner Mongolia.

6. Conclusions

The research analyzes the correlation and temporal–spatial variation characteristics of temperature and extreme precipitation indicators at various stations in Inner Mongolia from 1960 to 2019. The following conclusions can be drawn from this study.

- (1) The PRCPTOT and SDII researched in this work exhibited spatial distribution characteristics of more significant in the southeast and more minor in the northwest. In terms of the spatial distribution characteristics of wet days, the larger values are concentrated in Northeastern Inner Mongolia.
- (2) The Granger cause tests of the temperature and extreme precipitation indicators showed a correlation between each indicator and temperature at the significance level of 1%. The temperature had a positive correlation with only SDII, while the negative correlation with the remaining indicators and temperature was highly negatively correlated with wet days.
- (3) Regarding development trends of temperature and extreme precipitation indicators, there are mainly two types of relationships in Inner Mongolia. The first relationship (with the increase in temperature and the decrease in PRCPTOT and wet days) means an increase in drought disasters. The other type of relationship (an increase in SDII, along with an increase in temperature) means an increased risk in flood disaster events.

Author Contributions: Conceptualization, W.Z. and P.L.; Data curation, W.Z. and X.Z.; Formal analysis, W.Z.; Funding acquisition, P.L.; Investigation, W.Z.; Methodology, W.Z.; Resources, P.L.; Software, S.W.; Supervision, P.L., J.L., M.Z., B.H. and D.N.; Validation, W.Z. and Z.C.; Visualization, W.Z.; Writing—original draft, W.Z.; and Writing—review and editing, W.Z. All authors have read and agreed to the published version of the manuscript.

Funding: This study was supported by National Key R&D Program of China (2018YFE0103800); the Fundamental Research Funds for the Central Universities, CHD (300102299302, 300102299102, and 300102299104); International Collaborative Research of Disaster Prevention Research Institute of Kyoto University (2019W-02); One Hundred Talent Plan of Shaanxi Province; excellent projects for science and technology activities of overseas staff in Shaanxi Province (2018038); Special funds of education and teaching reform for the Central Universities of China (310629172112); the GDAS Project of Science and Technology Development (2020GDASYL-20200102013, 2020GDASYL-20200301003, 2020GDASYL-20200402003, and 2019GDASYL-0102002); experimental research on water conservancy science and a technology promotion project of the Water Conservancy Bureau of Gansu Province (2019-08, 2020-46, and 2021-71); Guangdong Foundation for the Program of Science and Technology Research (Grant No.2019B121205006); and the National Natural Science Foundation of China (51869023 and 41930865).

Institutional Review Board Statement: Not applicable.

Informed Consent Statement: Not applicable.

Data Availability Statement: The precipitation and temperature data were collected from Daily Terrestrial Climatological Dataset in China (V3.0) released by the National Meteorological Information Center (<http://data.cma.cn/>, accessed on 16 September 2021).

Acknowledgments: We appreciate the reviewers for providing valuable comments.

Conflicts of Interest: The authors declare no conflict of interest. The funders had no role in the study design, data collection, and analysis; decision to publish; or preparation of the manuscript.

References

- Haddeland, I.; Heinke, J.; Biemans, H.; Eisner, S.; Florke, M.; Hanasaki, N.; Wisser, D. Global water resources affected by human interventions and climate change. *Proc. Natl. Acad. Sci. USA* **2014**, *111*, 3251–3256. [[CrossRef](#)] [[PubMed](#)]
- Wei, L.H.; Gu, X.H.; Kong, D.D.; Liu, J.Y. A long-term perspective of hydroclimatological impacts of tropical cyclones on regional heavy precipitation over eastern monsoon China. *Atmos. Res.* **2021**, *264*, 105862. [[CrossRef](#)]
- Blanchet, J.; Ceresetti, D.; Molinié, G.; Creutin, J.-D. A regional GEV scale-invariant framework for Intensity–Duration–Frequency analysis. *J. Hydrol.* **2016**, *540*, 82–95. [[CrossRef](#)]
- Ghanmi, H.; Bargaoui, Z.; Mallet, C. Estimation of intensity-duration-frequency relationships according to the property of scale invariance and regionalization analysis in a Mediterranean coastal area. *J. Hydrol.* **2016**, *541*, 38–49. [[CrossRef](#)]
- AghaKouchak, A.; Cheng, L.Y.; Mazdiyasn, O.; Farahmand, A. Global warming and changes in risk of concurrent climate extremes: Insights from the 2014 California drought. *Geophys. Res. Lett.* **2014**, *41*, 8847–8852. [[CrossRef](#)]
- Pöschmann, J.M.; Kim, D.; Kronenberg, R.; Bernhofer, C. An analysis of temporal scaling behaviour of extreme rainfall in Germany based on radar precipitation QPE data. *Nat. Hazards Earth Syst. Sci.* **2021**, *21*, 1195–1207. [[CrossRef](#)]
- Nigussie, T.A.; Altunkaynak, A. Impacts of climate change on the trends of extreme rainfall indices and values of maximum precipitation at Olimpiyat Station, Istanbul, Turkey. *Theor. Appl. Climatol.* **2019**, *135*, 1501–1515. [[CrossRef](#)]
- Moberg, A.; Jones, P.D. Trends in indices for extremes in daily temperature and precipitation in central and western Europe, 1901–1999. *Int. J. Climatol. A J. R. Meteorol. Soc.* **2005**, *25*, 1149–1171. [[CrossRef](#)]
- Santos, C.A.C.D. Recent changes in temperature and precipitation extremes in an ecological reserve in Federal District, Brazil. *Rev. Bras. Meteorol.* **2014**, *29*, 13–20. [[CrossRef](#)]
- Easterling, D.R.; Meehl, G.A.; Parmesan, C.; Changnon, S.A.; Karl, T.R.; Mearns, L.O. Climate extremes: Observations, modeling, and impacts. *Science* **2000**, *289*, 2068–2074. [[CrossRef](#)]
- Aihaiti, A.; Jiang, Z.H.; Zhu, L.H.; Li, W.; You, Q.L. Risk changes of compound temperature and precipitation extremes in China under 1.5 degrees C and 2 degrees C global warming. *Atmos. Res.* **2021**, *64*, 105838. [[CrossRef](#)]
- Luo, P.; Mu, Y.; Wang, S.; Zhu, W.; Mishra, B.K.; Huo, A.; Zhou, M.; Lyu, J.; Hu, M.; Duan, W. Exploring sustainable solutions for the water environment in Chinese and Southeast Asian cities. *Ambio* **2022**, *51*, 1199–1218. [[CrossRef](#)] [[PubMed](#)]
- Luo, P.; Xu, C.; Kang, S.; Huo, A.; Lyu, J.; Zhou, M.; Nover, D. Heavy metals in water and surface sediments of the Fenghe River Basin, China: Assessment and source analysis. *Water Sci. Technol.* **2021**, *84*, 3072–3090. [[CrossRef](#)] [[PubMed](#)]
- Zha, X.; Luo, P.; Zhu, W.; Wang, S.; Lyu, J.; Zhou, M.; Huo, A.; Wang, Z. A bibliometric analysis of the research on Sponge City: Current situation and future development direction. *Ecohydrology* **2021**, *14*, e2328. [[CrossRef](#)]
- Easterling, D.R.; Alexander, L.V.; Mokssit, A.; Detemmerman, V. CCI/CLIVAR workshop to develop priority climate indices. *Bull. Am. Meteorol. Soc.* **2003**, *84*, 1403–1407. [[CrossRef](#)]
- Hao, Z.; AghaKouchak, A.; Phillips, T.J. Changes in concurrent monthly precipitation and temperature extremes. *Environ. Res. Lett.* **2013**, *8*, 034014. [[CrossRef](#)]
- Folland, C.K.; Rayner, N.A.; Brown, S.; Smith, T.; Shen, S.; Parker, D.; Nicholls, N. Global temperature change and its uncertainties since 1861. *Geophys. Res. Lett.* **2001**, *28*, 2621–2624. [[CrossRef](#)]

18. Zscheischler, J.; Orth, R.; Seneviratne, S.I. Bivariate return periods of temperature and precipitation explain a large fraction of European crop yields. *Biogeosciences* **2017**, *14*, 3309–3320. [[CrossRef](#)]
19. Yihui, D.; Chan, J.C. The East Asian summer monsoon: An overview. *Meteorol. Atmos. Phys.* **2005**, *89*, 117–142. [[CrossRef](#)]
20. You, Q.L.; Kang, S.C.; Aguilar, E.; Pepin, N.; Flugel, W.A.; Yan, Y.P.; Huang, J. Changes in daily climate extremes in China and their connection to the large scale atmospheric circulation during 1961–2003. *Clim. Dyn.* **2011**, *36*, 2399–2417. [[CrossRef](#)]
21. Wang, S.; Gong, D. Enhancement of the warming trend in China. *Geophys. Res. Lett.* **2000**, *27*, 2581–2584. [[CrossRef](#)]
22. Zhai, P.; Zhang, X.; Wan, H.; Pan, X. Trends in total precipitation and frequency of daily precipitation extremes over China. *J. Clim.* **2005**, *18*, 1096–1108. [[CrossRef](#)]
23. Almazroui, M.; Saeed, S. Contribution of extreme daily precipitation to total rainfall over the Arabian Peninsula. *Atmos. Res.* **2020**, *231*, 104672. [[CrossRef](#)]
24. Tong, S.; Li, X.; Zhang, J.; Bao, Y.; Bao, Y.; Na, L.; Si, A. Spatial and temporal variability in extreme temperature and precipitation events in Inner Mongolia (China) during 1960–2017. *Sci. Total Environ.* **2019**, *649*, 75–89. [[CrossRef](#)] [[PubMed](#)]
25. Khan, R.S.; Bhuiyan, M.A.E. Artificial intelligence-based techniques for rainfall estimation integrating multisource precipitation datasets. *Atmosphere* **2021**, *12*, 1239. [[CrossRef](#)]
26. Derin, Y.; Yilmaz, K.K. Evaluation of multiple satellite-based precipitation products over complex topography. *J. Hydrometeorol.* **2014**, *15*, 1498–1516. [[CrossRef](#)]
27. Mei, Y.; Nikolopoulos, E.I.; Anagnostou, E.N.; Borga, M. Evaluating satellite precipitation error propagation in runoff simulations of mountainous basins. *J. Hydrometeorol.* **2016**, *17*, 1407–1423. [[CrossRef](#)]
28. Aihua, M.; Dapeng, Y.; Jingbo, Z. Spatiotemporal variation and effect of extreme precipitation in Inner Mongolia in recent 60 years. *Arid Zone Res.* **2020**, *37*, 74–85. [[CrossRef](#)]
29. Peng, Y.; Long, S.; Ma, J.; Song, J.; Liu, Z. Temporal-spatial variability in correlations of drought and flood during recent 500 years in Inner Mongolia, China. *Sci. Total Environ.* **2018**, *633*, 484–491. [[CrossRef](#)]
30. Li, Y.; Xin-Gang, D.; Yu, Z. Extreme precipitation events in Inner Mongolia in 1961–2008. *Adv. Clim. Change Res.* **2010**, *6*, 411.
31. Wei, X.; Wang, N.; Luo, P.; Yang, J.; Zhang, J.; Lin, K. Spatiotemporal assessment of land marketization and its driving forces for sustainable urban–rural development in Shaanxi province in China. *Sustainability* **2021**, *13*, 7755. [[CrossRef](#)]
32. Wang, Q.; Zhang, M.J.; Wang, S.J.; Ma, Q.; Sun, M.P. Changes in temperature extremes in the Yangtze River Basin, 1962–2011. *J. Geogr. Sci.* **2014**, *24*, 59–75. [[CrossRef](#)]
33. Costa, A.C.; Soares, A. Trends in extreme precipitation indices derived from a daily rainfall database for the South of Portugal. *Int. J. Climatol. A J. R. Meteorol. Soc.* **2009**, *29*, 1956–1975. [[CrossRef](#)]
34. Trambly, Y.; El Adlouni, S.; Servat, E. Trends and variability in extreme precipitation indices over Maghreb countries. *Nat. Hazards Earth Syst. Sci.* **2013**, *13*, 3235–3248. [[CrossRef](#)]
35. Bhatti, A.S.; Wang, G.; Ullah, W.; Ullah, S.; Fiifi Tawia Hagan, D.; Kwesi Nooni, I.; Ullah, I. Trend in extreme precipitation indices based on long term in situ precipitation records over Pakistan. *Water* **2020**, *12*, 797. [[CrossRef](#)]
36. Fahimnia, B.; Sarkis, J.; Davarzani, H. Green supply chain management: A review and bibliometric analysis. *Int. J. Prod. Econ.* **2015**, *162*, 101–114. [[CrossRef](#)]
37. Sims, C.A. Macroeconomics and reality. *Econom. J. Econom. Soc.* **1980**, *48*, 1–48. [[CrossRef](#)]
38. Abrigo, M.R.; Love, I. Estimation of panel vector autoregression in Stata. *Stata J.* **2016**, *16*, 778–804. [[CrossRef](#)]
39. Levin, A.; Lin, C.-F.; Chu, C.-S.J. Unit root tests in panel data: Asymptotic and finite-sample properties. *J. Econom.* **2002**, *108*, 1–24. [[CrossRef](#)]
40. Im, K.S.; Pesaran, M.H.; Shin, Y. Testing for unit roots in heterogeneous panels. *J. Econom.* **2003**, *115*, 53–74. [[CrossRef](#)]
41. Breitung, J.; Das, S. Panel unit root tests under cross-sectional dependence. *Stat. Neerl.* **2005**, *59*, 414–433. [[CrossRef](#)]
42. Choi, I. Unit root tests for panel data. *J. Int. Money Financ.* **2001**, *20*, 249–272. [[CrossRef](#)]
43. Westerlund, J. A note on the use of the LLC panel unit root test. *Empir. Econ.* **2009**, *37*, 517–531. [[CrossRef](#)]
44. Maddala, G.S.; Wu, S. A comparative study of unit root tests with panel data and a new simple test. *Oxf. Bull. Econ. Stat.* **1999**, *61*, 631–652. [[CrossRef](#)]
45. Andrews, D.W.; Lu, B. Consistent model and moment selection procedures for GMM estimation with application to dynamic panel data models. *J. Econom.* **2001**, *101*, 123–164. [[CrossRef](#)]
46. Sassi, S.; Gasmi, A. The Dynamic Relationship Between Corruption—Inflation: Evidence from Panel Vector Autoregression. *Jpn. Econ. Rev.* **2017**, *68*, 458–469. [[CrossRef](#)]
47. Childs, C. Interpolating surfaces in ArcGIS spatial analyst. *ArcUser* **2004**, *3235*, 32–35.
48. Meng, Q.; Liu, Z.; Borders, B.E. Assessment of regression kriging for spatial interpolation—comparisons of seven GIS interpolation methods. *Cartogr. Geogr. Inf. Sci.* **2013**, *40*, 28–39. [[CrossRef](#)]
49. Siska, P.P.; Hung, I.-K. Assessment of kriging accuracy in the GIS environment. In Proceedings of the 21st Annual ESRI International Conference, San Diego, CA, USA, 9–13 July 2001.
50. Kendall, M.G. A new measure of rank correlation. *Biometrika* **1938**, *30*, 81–93. [[CrossRef](#)]
51. Mann, H.B. Nonparametric tests against trend. *Econom. J. Econom. Soc.* **1945**, *13*, 245–259. [[CrossRef](#)]
52. Sen, P.K. Estimates of the regression coefficient based on Kendall’s tau. *J. Am. Stat. Assoc.* **1968**, *63*, 1379–1389. [[CrossRef](#)]
53. Xie, S.; Liu, Y.; Yao, F. Spatial Downscaling of TRMM Precipitation Using an Optimal Regression Model with NDVI in Inner Mongolia, China. *Water Resour.* **2020**, *47*, 1054–1064. [[CrossRef](#)]

54. Mukherjee, S.; Aadhar, S.; Stone, D.; Mishra, V. Increase in extreme precipitation events under anthropogenic warming in India. *Weather Clim. Extrem.* **2018**, *20*, 45–53. [[CrossRef](#)]
55. Higgins, R.; Schemm, J.E.; Shi, W.; Leetmaa, A. Extreme precipitation events in the western United States related to tropical forcing. *J. Clim.* **2000**, *13*, 793–820. [[CrossRef](#)]
56. Li, W.; Jiang, Z.; Zhang, X.; Li, L. On the emergence of anthropogenic signal in extreme precipitation change over China. *Geophys. Res. Lett.* **2018**, *45*, 9179–9185. [[CrossRef](#)]
57. Reynolds, J.F.; Smith, D.M.S.; Lambin, E.F.; Turner, B.; Mortimore, M.; Batterbury, S.P.; Herrick, J.E. Global desertification: Building a science for dryland development. *Science* **2007**, *316*, 847–851. [[CrossRef](#)]
58. Wei, X.; Yang, J.; Luo, P.; Lin, L.; Lin, K.; Guan, J. Assessment of the variation and influencing factors of vegetation NPP and carbon sink capacity under different natural conditions. *Ecol. Indic.* **2022**, *138*, 108834. [[CrossRef](#)]